Geo-Marine Letters (2025) 45:41
https://doi.org/10.1007/s00367-025-00830-8

RESEARCH

Large-scale methane venting and clathrite-like structures recorded in the late Miocene foredeep deposits of the northern Apennines (Marnoso-arenacea Fm, Italy)

Simone Muzzioli[1] · Stefano Conti[1] · Claudio Argentino[2] · Daniela Fontana[1]

Received: 26 June 2025 / Accepted: 27 October 2025

Abstract

Ancient methane seep deposits exposed in the Apennine mountains of northern Italy are key to reconstruct the geodynamic evolution of the Miocene foredeep basin prior to the Messinian Salinity Crisis. Here, we report on a new Miocene outcrop of seep-carbonates in the Romagna region which showed indications of paleo-gas hydrate destabilization. We combined carbonate facies analyses, petrography of thin sections, scanning-electron microscopy and stable isotope analyses to interpret the origin of these authigenic carbonates and biogeochemical conditions at the time of their formation. These deposits show vuggy, brecciated and massive-with-lucinids facies and are characterized by light carbon isotope signatures, as negative as −47.8‰. The oxygen isotope compositions of these carbonates are out of equilibrium with coeval bottom seawater, exhibiting anomalously-heavy values. We calculated the stability of paleo-gas hydrates, which revealed that gas hydrates type I (pure methane) were stable at depths > 480 m, in agreement with the paleo-bathymetric domain of this outcrop. This area was geologically active in the Late Miocene and affected by continuous bathymetric changes caused by the eastwardly-migrating accretionary wedge and foredeep basin. We propose that gas hydrate destabilization and prolonged anaerobic oxidation of methane in the shallow sediment produced the studied carbonate deposits.

Introduction

In marine environments, subsurface hydrocarbon generation, migration and seafloor emission lead to the formation of cold seeps, which are sites where hydrocarbon-charged fluids are released into the water column (Campbell 2006) and potentially reach the atmosphere (Weber et al. 2019). Distinct features of submarine hydrocarbon emissions are a lush chemosymbiotic macrofauna (Dubilier et al. 2008) and authigenic carbonates, formed by microbially-mediated anaerobic oxidation of methane (Boetius et al. 2000; Luff et al. 2004). These carbonates, hereafter named seep-carbonates, are typified by a distinct geochemical composition which is particularly depleted in ^{13}C, due to incorporation of methane-derived carbon (Luff and Wallmann 2003; Peckmann and Thiel 2004; Cochran et al. 2022). The dynamic nature of cold seeps contributes to the variability in the morphology, size and distribution of seep-carbonates (Jakubowicz et al. 2020) as well as of the chemosynthetic habitats at the seafloor (Levin 2005; Judd and Hovland 2009). Moderate methane fluxes favor the precipitation of carbonates (Aloisi et al. 2000) and sustain widespread chemosynthetic communities including microbial mats, tubeworms and bivalves, disposed in a concentric zonation around the seep or forming chemoherm-type build-ups (Roberts 2001; Taludaker 2012; Ho et al. 2012). Conversely, high flow rates inhibit benthic macrofauna to a large extent due to toxicity of sulfide released by AOM, while favoring the development of seafloor depressions such as pockmarks and larger craters in low permeability sediments (Judd and Hovland 2009). Seep-carbonates associated with seafloor mounds have been reported from gas hydrate pingoes (Serov et al. 2017) and mud volcanoes (Loher et al. 2018; Panieri et al. 2025; Argentino et al. 2025) and often display brecciated facies and typical vuggy fabric, multiple cement generations and chaotic arrangements of fractures and veins. These structures are indicative of high-energy conditions during seep-carbonate growth and, together with anomalously-heavy oxygen isotope signatures ($\delta^{18}O$), can

✉ Claudio Argentino
claudio.argentino@uit.no

[1] Department of Chemical and Geological Sciences, University of Modena and Reggio Emilia, Modena, Italy

[2] Department of Geosciences, UiT The Arctic University of Norway, Tromsø, Norway

Published online: 10 November 2025

be proxies for gas-hydrate dissociation (Bohrmann et al. 2002; Teichert et al. 2005; Bohrmann and Torres 2006). Gas hydrate dissociation releases ^{18}O-enriched fresh water and methane into sediments, thus affecting the bulk stable oxygen isotopic composition of seep-carbonates (Naehr et al. 2007; Tong et al. 2016; Han et al. 2014; Loyd et al. 2016). Gas hydrate-associated carbonates, also known as clathrites, generally form bodies of large dimension and show peculiar structures and lithologies (Kennett and Fackler-Adams 2000), relatively well described in modern seep settings (Bohrmann and Torres 2006; Abegg et al. 2007): carbonate crusts growing within pure gas hydrate layers oriented parallel to the bedding surfaces, vacuolar structures that mimics the shape of gas hydrate bubbles, associations of pure aragonitic and gas hydrate layers (zebra-like structures), monomictic and polimictic breccias resulting from the rapid destabilization of gas hydrates formerly present within the sediment pore spaces. Following present-day analogues, the possible role of gas hydrates in the formation of fossil seep-carbonates can the deduced by textural and geochemical ($\delta^{18}O$) proxies applied in several studies in the Oligocene and Miocene of the Apennine and Carpathian chains (Dela Pierre et al. 2010; Argentino et al. 2019a; Conti et al. 2021; Bojanowski et al. 2021).

Fossil seep-carbonates are therefore crucial in reconstructing the style and magnitude of past fluid circulation through the upper crust with implications for geodynamic and past atmosphere composition (Hryniewicz 2022). In the northern Apennines of Italy, the late Miocene paleo-tectonic and paleo-environmental context is particularly debated due to the complex relationships among tectonics, climatic changes and sea level drops, (Di Giulio et al. 2013; Conti et al. 2024) with different and contrasting reconstructions which may be improved by the analyses of the numerous Tortonian to Messinian seep-carbonates outcrops. Here, Messinian seep-carbonates are often strongly brecciated with vuggy fabric and authigenic micrite depleted in ^{13}C and enriched in ^{18}O, as expected during hydrate destabilization. In this study we investigated for the first time the well exposed outcrops of seep-carbonates contained within the Late Miocene foredeep deposits of the Romagna Apennines in the Predappio area (northern Italy) (Fig. 1). They are of special importance for highlighting the occurrence of paleo gas-hydrates in deep marine environments prior to the Mediterranean desiccation.

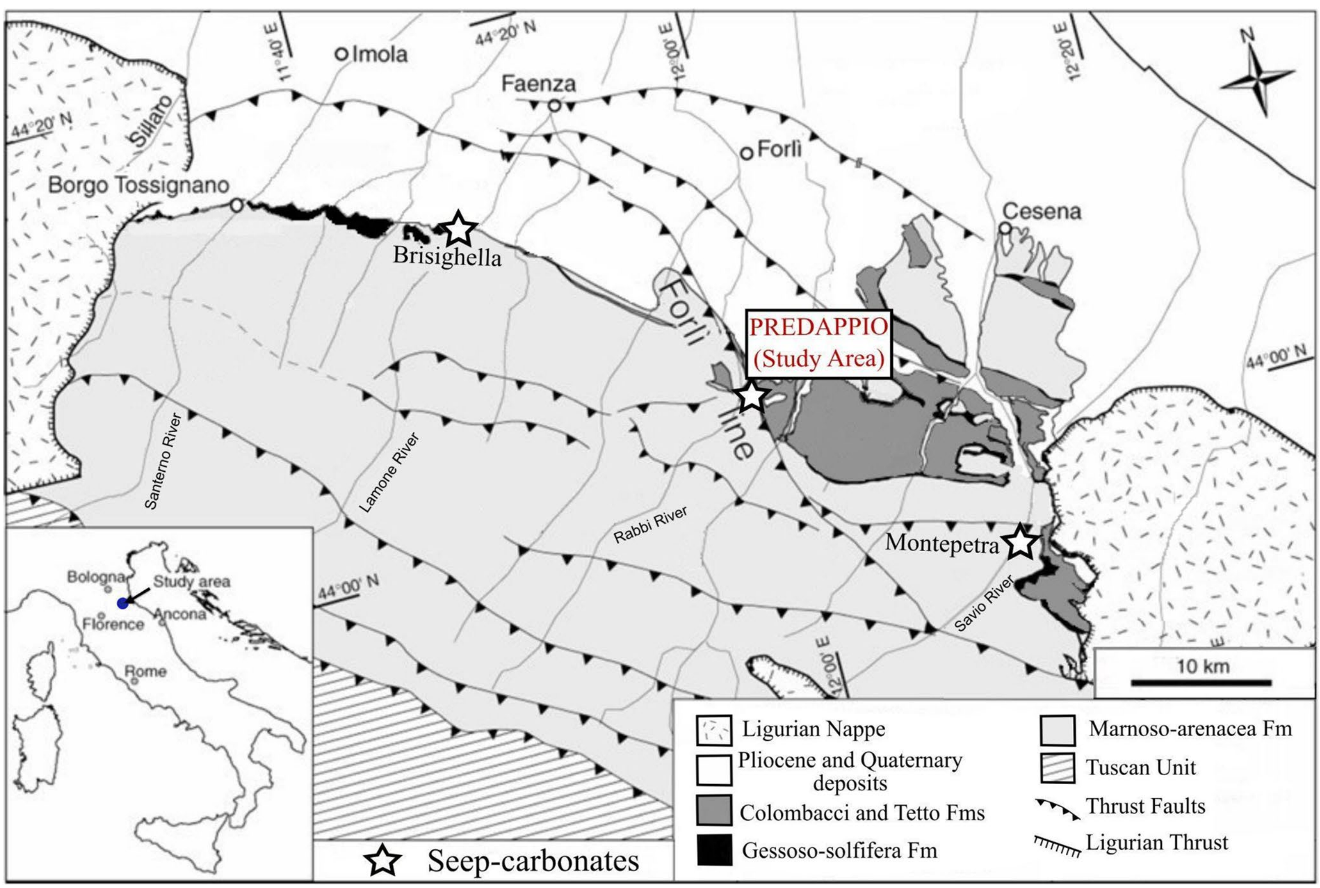

Fig. 1 Simplified structural map of the Romagna Apennines (Italy) showing the location of the studied outcrops (Predappio area) in relation to the main structural elements and geological domains. Modified after Bonini (2006)

Geological setting

The northern Apennine chain consists of several imbricated tectonic units bound by thrusts generally verging to the northeast, formed since Late Eocene-early Oligocene for the convergence between the European and African plates. The orogenic wedge developed on top of the subducting and retreating Adria plate, flexing and progressively embedding the adjacent foredeep basin (Le Breton et al. 2017). Deposition mainly occurred in wedge-top and in the foredeep basin filled by the thick turbidite succession of the Miocene Marnoso-arenacea Formation (Fm) (Argnani and Ricci Lucchi 2001; Faccenna et al. 2001; Conti et al. 2016). In the Langhian-Messinian, during the migration of the thrust-front, foredeep siliciclastic deposits were incorporated in the accretionary wedge causing the closure of the foredeep. The closure stage is marked by silty-clayey hemipelagic slope mudstones, sporadic channelized arenaceous bodies and organic-rich mudstones informally named euxinic shales. These deposits enclose numerous seep-carbonate bodies, lens-like to stratiform, late Tortonian to early Messinian in age (Terzi et al. 1994; Conti et al. 2008). Seep-carbonates formed in different settings and have various morphologies: - isolated blocks with a metric extension included in poorly cemented sandstones deposited in submarine canyons; - large (up to 100 m) stratiform bodies included in fine-grained apron sediments over the slope; - lenticular to stratiform bodies (1–100 m long) in restricted basins hosted in euxinic shales draping thrust bounded faults and buried ridges, forming intrabasinal highs (Ghioli di letto mudstones referring to the closure stage of the Marnoso-arenacea Fm foredeep) (Argentino et al. 2019a; Conti et al. 2024). The Messinian succession passes upward with evaporitic deposits of the Gessoso-solfifera Fm, consisting of up to 16 massive gypsum beds, about 30 m thick, made of both primary (selenitic) and clastic (gypsarenitic) gypsum (Lugli et al. 2007). The passage to the evaporites is marked by 2 m-thick laminated brown to white carbonates (Calcare di Base *auctorum*) interpreted in many outcrops of microbial origin (Guido et al. 2007) and recently interpreted locally as being methane-derived carbonates (Conti et al. 2024). The carbonate outcrop investigated in our study pertains to this context and is a new case to determining the temporal and spatial scales of cold seepage prior to the Messinian Salinity Crisis. In the studied area the Messinian succession ends with the discordant, erosive fluvio-deltaic and lacustrine deposits with brackish water fauna of the Lago-Mare biofacies (Bassetti et al. 2004), ascribed to various continental and transitional environments. Climatic oscillations and tectonics determined the evolution from brackish "lake-sea" to marginal fluvio-deltaic and marsh conditions (Lugli et al. 2007).

Methods

A detailed field work of the Predappio area has allowed us to draft a 1:5.000 geological map (Fig. 2) including the distribution, facies and geometries of seep-carbonates. A stratigraphic log, 30 m thick (Fig. 3), was measured in detail in the well-exposed Sasseto outcrops where seep-carbonates exhibit different facies and are covered with erosive contact by conglomerates of the Colombacci Fm. We distinguished lithology, fossil content, depositional and fluid related structures, focusing more on the brecciated and vuggy fabrics due to their significance in relation to paleo-seep dynamics. Eleven samples of carbonate rocks, subdivided in 29 sub-samples, were sampled from all facies (Figs. 2 and 3; Table 1) for petrographic and isotopic analyses in order to identify different microfacies and authigenic phases (sample SM1 was not analyzed as partially altered). Five marly samples (SM2, SM4, SM5, SM6, SM7) were collected in the hosting sediments near the contact with carbonate bodies (Fig. 2) and analyzed for nannofossil biostratigraphy. Thin sections were studied using a Leitz optical microscope and investigated via Scanning Electron Microscopy hosted at the Department of Chemical and Geological Sciences, University of Modena and Reggio Emilia (Italy); semi-quantitative elemental information were acquired via energy-dispersive spectrometry (EDS) at accelerating voltage of 20 kV and spot size 60 mm. SEM-EDS analyses were focused on three samples (PR8, PR9, PR10) collected from a brecciated and vuggy carbonate facies. Results are reported in the Supplementary Information. Material for stable C and O isotope analysis was collected from the microcrystalline groundmass, and from different cement phases: 18 powder samples of carbonates, massive and laminated, were analyzed at the Department of Chemical, Life and Environmental Sustainability of the University of Parma. About 10 mg were reacted with 100% phosphoric acid at 25 °C for 24 h. The purified CO_2 gas was analyzed using a Finnigan MAT 252 gas isotope ratio mass spectrometer. Replicate analyses of reference materials throughout the session yielded a precision better than 0.1‰ (1s; $n=3$) for both $\delta^{13}C$ and $\delta^{18}O$ values. A second batch of 11 powders were prepared and analyzed at the University of Modena and Reggio Emilia. Powders were obtained using a handheld microdrill from thin section slabs or polished rock surfaces. Around 0.5 mg were reacted with 100% phosphoric acid at 25 °C for ~4 h. The purified gas was analyzed on a Isoprime precisION (Elementar) stable isotope ratio mass spectrometer at Centro Interdipartimentale Grandi Strumenti (C.I.G.S.) of the University of Modena e Reggio Emilia. The signal was checked until a stable response was observed to ensure complete sample digestion. Accuracy of the measurements was evaluated by running six replicates of both NBS18 and

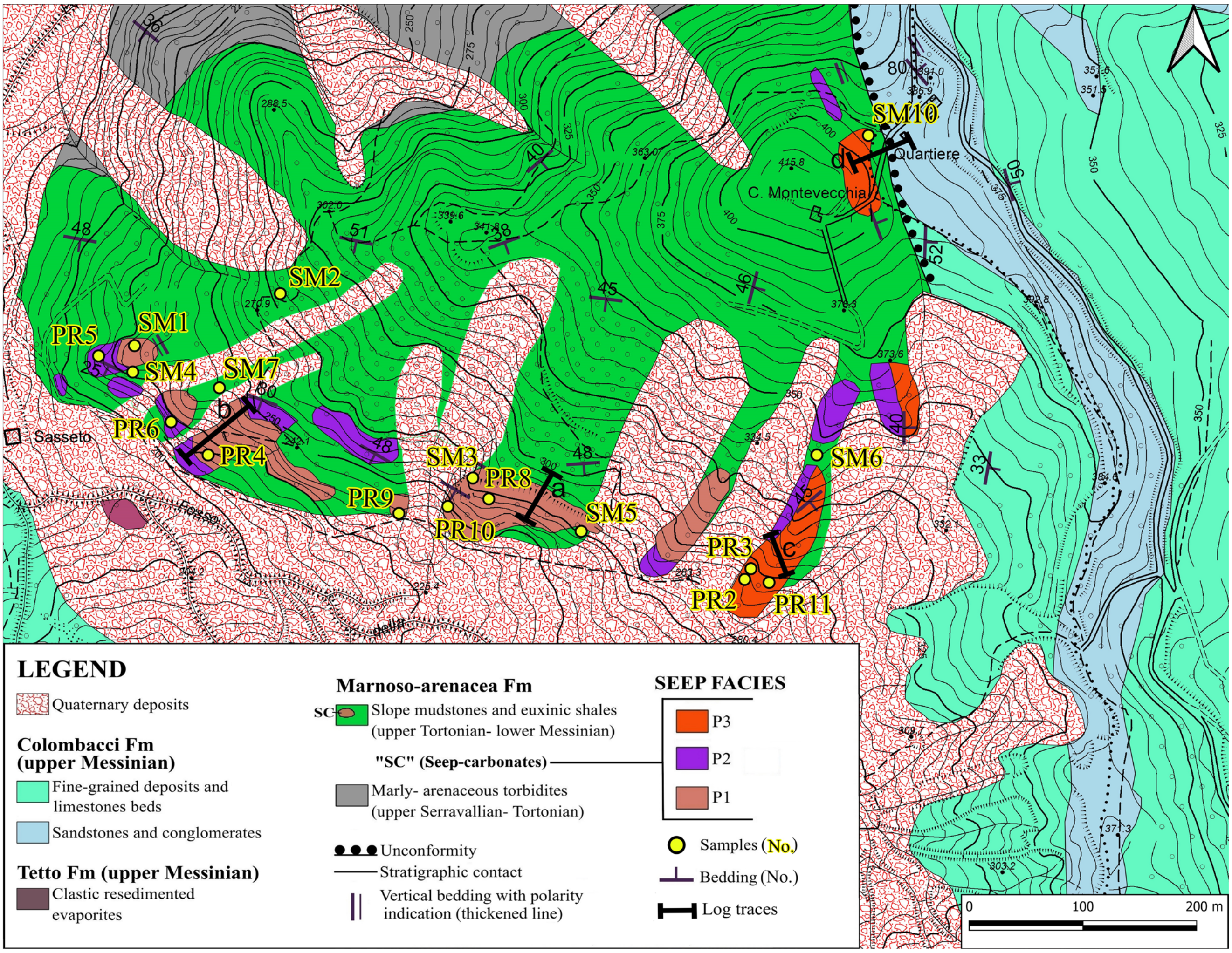

Fig. 2 Detailed geological map of the studied carbonate outcrops near Sasseto in the Predappio area showing seep facies distribution and enclosing rocks: at the base, slope mudstones and euxinic shales of the upper Miocene Marnoso-arenacea Fm and overlying conglomerates of the upper Messinian Colombacci Fm. The location of the collected samples is reported (yellow color); samples SM 2, 4, 5, 6, 7 were used exclusively for nannofossil analysis. The numbers adjacent to the bedding symbol refer to the dip angle. The strike of the unconformity in the upper right runs parallel to the direction of the Forlì Line (Fig. 1). The source of the topographic map is Section no. 254,120, 1:10.000, Predappio sud (Regione Emilia Romagna)

NBS19 reference materials, yielding results in agreement with recommended values. Repeatability precision (1s) of three duplicate samples measured in the same session was better than 0.13‰ and 0.084‰ for $\delta^{13}C$ and $\delta^{18}O$, respectively. All isotope results are reported in standard δ notation relative to the Vienna-PeeDee Belemnite (V-PDB) standard.

Modelling of paleo-gas hydrate stability

Gas hydrate stability at the time of seep-carbonate formation is difficult to extrapolate since there remain uncertainties on the paleo-environmental conditions. However, we estimated the minimum paleo-seafloor depth at which gas hydrates were stable by assuming: (1) pure methane-hydrate (structure I); (2) normal salinity 37 psu (Flecker et al. 2015); (3) normal geothermal gradient 31 °C/km; (4) bottom water temperature = 5 °C (Barbieri et al. 2000); (5) steady state conditions. The model was implemented on the graphical user interface CAGEHYD (Vadakkepuliyambatta 2019) based on the CSMHYD code (Sloan 2006). Model results for different paleo-depths are reported in the Supplementary Information.

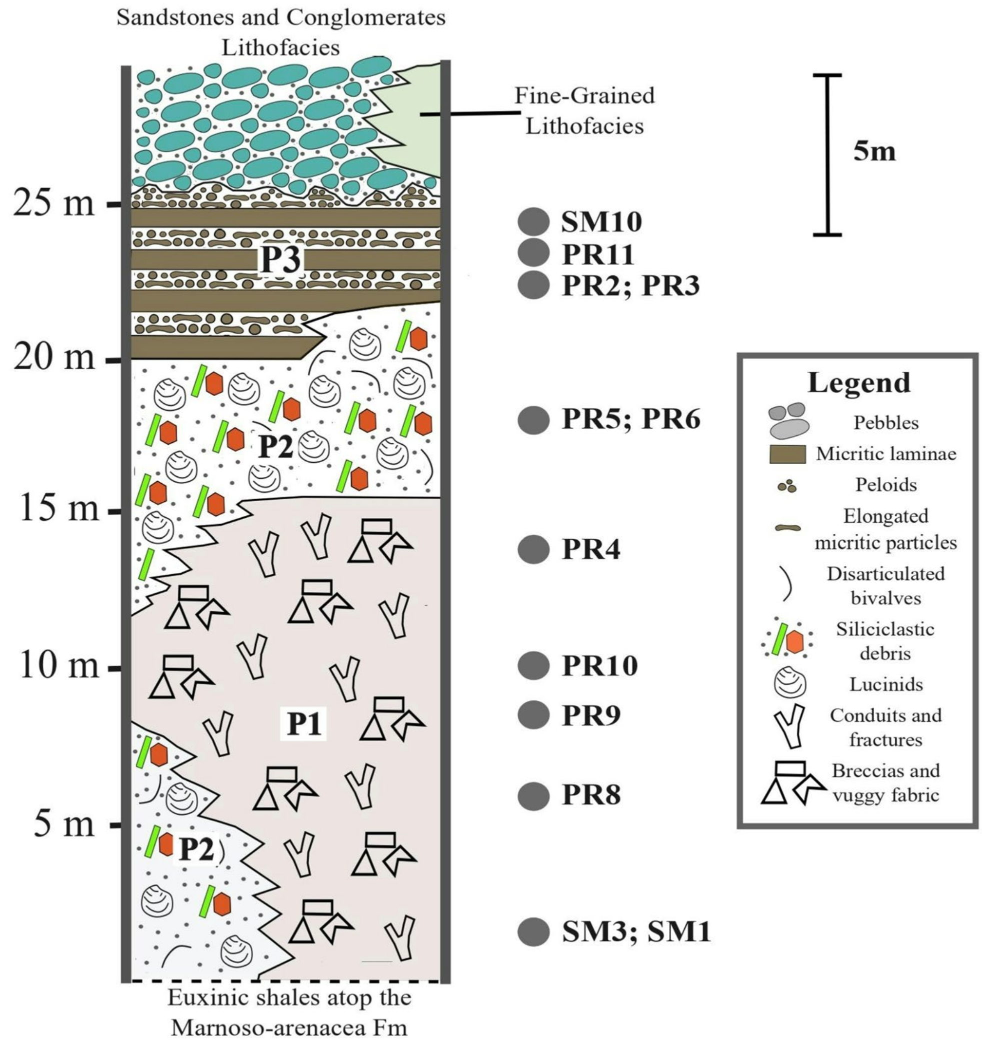

Fig. 3 Stratigraphic log of the Sasseto seep-carbonate outcrop (Predappio area) showing facies distribution, structures and samples. The base of the seep-carbonates is represented by euxinic shales of the Marnoso-arenacea Fm. Sandstones and conglomerates and fine-grained lithofacies up section belong to the Colombacci Fm (see Fig. 2)

Results

Outcrop geology

The examined outcrops (Sasseto) are characterized by numerous bodies of methane-derived carbonates distributed laterally over 800 m in the WNW-ESE direction, in correspondence with two important tectonic structures (Figs. 1 and 2): in the western area, the carbonate bodies are parallel to one of the major buried external fronts of the northern Apennines (where the Tortonian Marnoso-arenacea Fm overthrusts the upper Messinian deposits). The eastern part of the outcrop shows carbonate bodies aligned to the N-S direction and parallel to the still active Forlì Line. The Forlì Line has an N-S anti-apenninic direction (as shown in Figs. 1 and 2), and is made of different structural elements.

The carbonate bodies have variable geometries, morphologies and distribution varying from lenticular, amygdaloid, pinnacles, stratiform and scattered-irregular, with thickness of individual bodies from 2 m to up to 30 m and lateral extent up to 100 m. Stratiform carbonate bodies are concordant with the encasing deposits (bed attitude is reported in Fig. 2), except for the basal pinnacular contact which is almost vertical. The carbonate bodies form reliefs that stand out on the encasing marly sediments, separated by valley incisions along which landslide phenomena develop (Fig. 2). The studied area is folded into an anticlinal structure with the axis dipping towards SE.

In the Sasseto outcrops we measured a 30 m-thick stratigraphic composite section (traces a, b, c, d in Fig. 2) through the seep-carbonate bodies from the basal contact with the euxinic facies of the Marnoso-arenacea Fm to the upper discordant contact with alluvial conglomerate

Table 1 Carbonate mineralogy, δ^{13}C and δ^{18}O values, for samples from predappio area representing all three facies and different cements. These results correspond to plot in Fig. 7. Carbonate mineralogy was established by thin section petrography and SEM

Sample	Facies	Target phase	Predominant Mineralogy	δ^{13}C (‰)	δ^{18}O (‰)
SM10a	P3	Cement laminae	Calcite	−11.3	1.8
SM10b	P3	Peloidal laminae	Calcite	−14.5	1.8
PR11	P3	Microsparitic cement	Calcite	−34.8	−0.7
PR3a	P3	Micritic laminae	Dolomite > Calcite	−8.7	4.8
PR3b	P3	Peloidal laminae	Dolomite > Calcite	−28.1	2.7
PR2a	P3	Micritic laminae	Calcite	−23.1	3.8
PR2b	P3	Peloidal laminae	Calcite	−47.8	0.8
PR6	P2	Micrite	Dolomite	−27.0	5.6
PR5	P2	Micrite	Dolomite	−32.7	5.8
PR4	P1	Light micrite	Dolomite	−39.8	7.0
PR10a	P1	Rim cement	Dolomite	−41.6	1.5
PR10b	P1	Light micrite	Dolomite	−35.0	6.3
PR10c	P1	Light micrite	Dolomite	−35.9	6.5
PR10d	P1	Rim cement	Dolomite	−42.4	3.1
PR10e	P1	Vuggy micrite	Dolomite	−41.6	6.1
PR9a	P1	Light micrite	Dolomite	−39.5	7.2
PR9b	P1	Light micrite	Dolomite	−39.8	7.9
PR9c	P1	Light micrite	Dolomite	−39.7	7.9
PR9d	P1	Rim cement	Dolomite	−39.7	2.7
PR9e	P1	Sparitic cement	Calcite	−38.5	2.7
PR9f	P1	Dark micrite	Dolomite	−39.6	7.0
PR8a	P1	Light micrite	Dolomite	−36.7	6.3
PR8b	P1	Sparitic Cement	Calcite	−44.2	0.0
PR8c	P1	Sparitic Cement	Calcite	−39.6	−0.2
PR8d	P1	Light micrite	Dolomite	−41.1	7.7
PR8e	P1	Rim cement	Dolomite	−44.1	0.6
PR8f	P1	Sparitic cement	Calcite	−43.0	1.2
PR8g	P1	Dark micrite	Dolomite	−41.2	6.3
SM3	P1	Sparitic cement	Calcite	−31.2	0.1

deposits of the Colombacci Fm (Fig. 3). Seep-carbonates exhibit different facies from brecciated to massive and to microbial laminated carbonates, each characterized by distinct lithologies, textures, presence/absence of veins or fractures and fossil content (Fig. 4a, b, c, d). We observed an overall vertical trend in carbonate facies succession, which is recurrent in the examined area passing from one side of the outcrop to adjacent areas. Single carbonate bodies can, however, display facies variations both vertically and laterally. With respect to the age of carbonate bodies, nannofossils in the enclosing marls few meters below the base of the carbonate outcrops indicate a biozone MNN8b (Tortonian) and possibly a slightly younger age (late Tortonian) cannot be excluded based on the occurrence of *Discoaster pentaradiatus* (Muzzioli, master thesis). In the proximity of the studied outcrop (Predappio), the marls above the carbonates indicate an early Messinian age. These preliminary data indicate a late Tortonian-early Messinian age for seep-carbonates, correlated to Montepetra and Brisighella outcrops (Fig. 1).

Facies 1 (P1) is typified bycarbonate breccias composed of heterometric angular to subangular micritic clasts (Fig. 4c), from 1 to10 cm in size, with different colors from grey to brown. Clasts are chaotically dispersed in the authigenic micritic matrix or in a fine to medium-grained sandy matrix. Larger clasts derive from the amalgamation of smaller heterometric clasts, testifying multiple phases of fragmentation and cementation. Brecciated facies typically marks the basal portion of the carbonate bodies where this facies can be up to 15 m thick. Breccias are also found in the lateral portions of carbonate bodies; in this case is less intensely brecciated. Brecciated portions are crossed by a reticulate of veins and extensional fractures, from 1 to 2 mm to 2 cm in diameter. Veins show an irregular arrangement; in most cases they join together to form larger veins (1–2 cm). Frequently. elongated fractures merge into vuggy fabrics with cavities ranging from 1 to 3 cm (Fig. 4e, f). The abundance of veins and fractures of centimetric dimension may give to the carbonate masses the appearance of megabreccias. The vein infillings may contain coquina debris (shell fragments), coarse sand detritus and carbonate micro-breccias. In this facies the fossil content is scarce, represented by disarticulated clams and rare articulated lucinids, or absent. Micritic, mottled carbonates pervaded by irregular networks of veins and druses (from few mm up to 3 cm in diameter) and cut by millimetric-scale fractures are scattered.

Facies 2 (P2) consists of massive marly limestones, pale brown in colour, with abundant fossil content. Fossils are densely packed articulated and disarticulated bivalves, mostly lucinids (Fig. 4b), as irregularly distributed clusters, in several cases in life position. Fossils range from a few centimeters, up to fifteen cm in diameter. Facies 2 dominates in the intermediate portion of the carbonate bodies beneath the microbial laminated carbonates, but it can be present also in the basal portion, with heteropic contact with the brecciated facies P1. Typically, this facies has a maximum thickness of 5–7 m.

Facies 3 (P3) is characterized by laminated microbialitic-like carbonates composed of millimetric-scale alternations of brown-dark gray to light grey-whitish laminae (Fig. 4d). The laminate pattern is sub-horizontal to wavy; macrofossils are very scarce to absent. Facies 3 characterizes the upper portion of the section, with a thickness of about 5 m. It is cut by an erosive contact with fluvial conglomerates of the Colombacci Fm. Facies 3 locally is heteropic with stratified calcarenites with decimetric beds and occasional weak lamination.

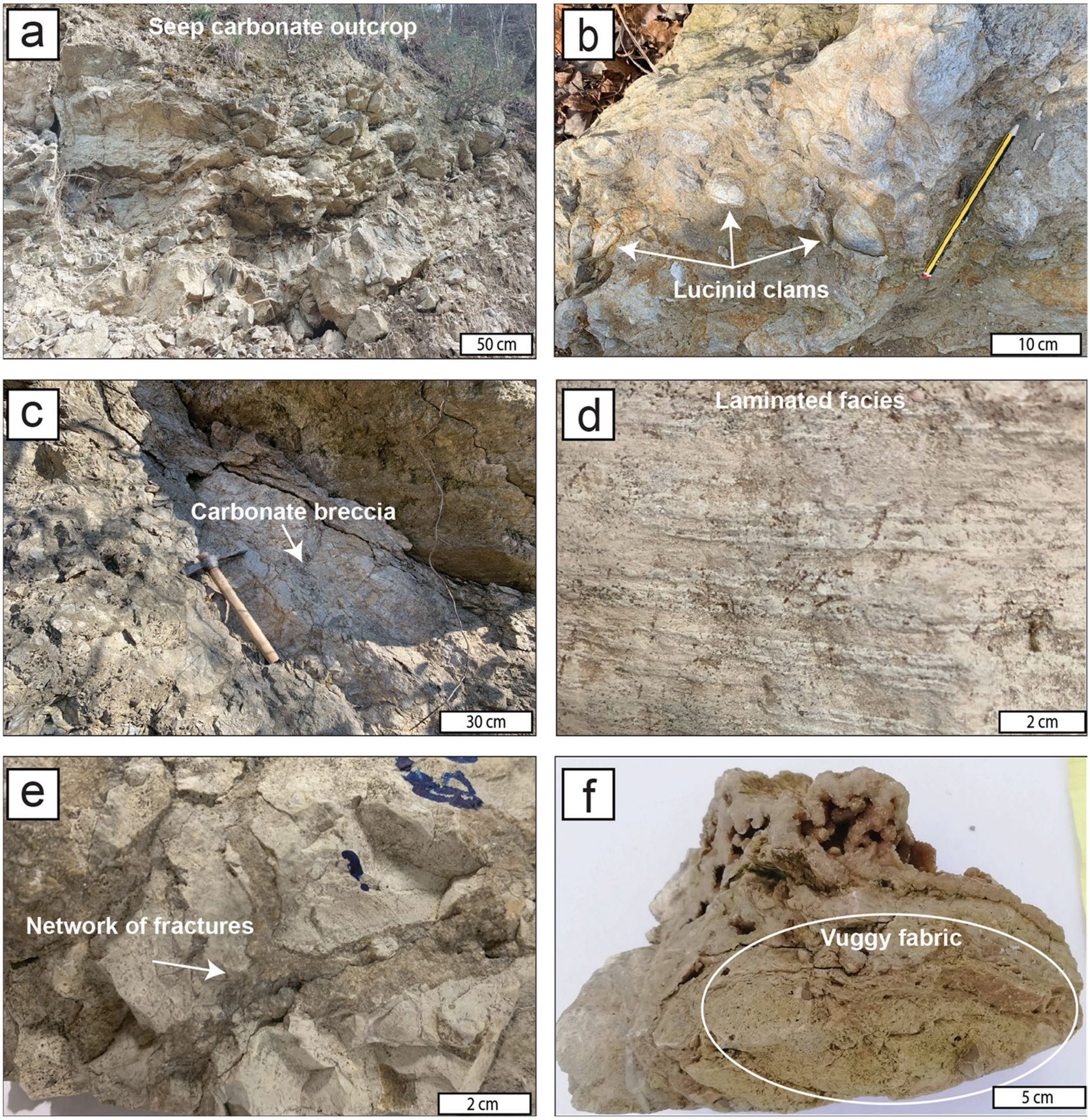

Fig. 4 Seep-carbonate facies in the studied outcrops: (**a**) stratiform seep-carbonate body containing abundant macrofauna; (**b**) densely packed lucinid-like clams in the P2 facies (**c**) carbonate monogenic breccias in the basal portion of the seep-carbonate sequence (P1); (**d**) laminated carbonates upsection (P3 facies); (**e**) network of fractures filled by authigenic micrite in the brecciated facies; (**f**) vuggy fabric with abundant microcavities showing an irregular elongated shape, oriented parallel to the bed/laminae surfaces, marked by a rim of dark dolomicrite (P1 facies)

Petrography

Samples from the massive facies with lucinid bivalves in the lower-middle part of the sections are predominantly made of micrite, forming a pervasive groundmass (Fig. 5a), with minor early-diagenetic microsparite (Fig. 5b) and later sparite. Micrite, light to dark in color, is composed of dolomite but calcite is also present (Table 1). Microspar may be calcitic and dolomitic. Massive micrite locally contains planktonic foraminifera as well as sand- to silt-sized

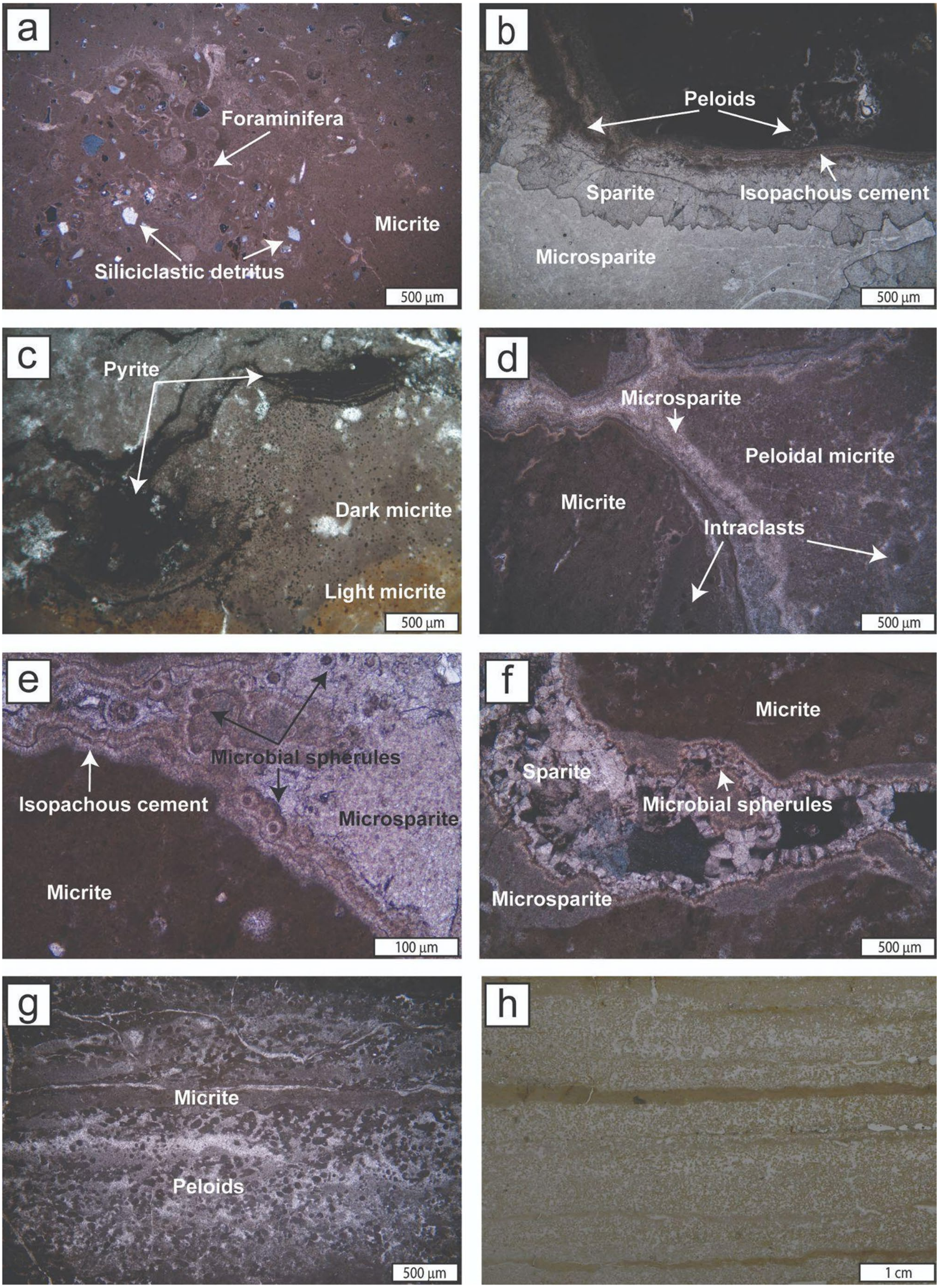
a
Foraminifera
Micrite
Siliciclastic detritus
500 µm
b
Peloids
Sparite
Isopachous cement
Microsparite
500 µm
c
Pyrite
Dark micrite
Light micrite
500 µm
d
Microsparite
Peloidal micrite
Micrite
Intraclasts
500 µm
e
Microbial spherules
Isopachous cement
Microsparite
Micrite
100 µm
f
Micrite
Sparite
Microbial spherules
Microsparite
500 µm
g
Micrite
Peloids
500 µm
h
1 cm

Fig. 5 Photomicrograph of the studied seep-carbonates: (**a**) micritic carbonates of the massive facies, made up of dolomite and subordinate calcite, locally containing planktonic foraminifera and silt-sized siliciclastic detrital material sourced from the underlying Marnoso-arenacea turbiditess; (**b**) Different generations of microsparitic to sparitic and isopachous cements bordering fractures in the massive facies; (**c**) Pyrite in dark dolomicrite of the massive facies forming patches of thin microbial laminae; light micrite in the lower right; (**d**) Different types of micritic intraclasts (dark micrite and peloidal) in the brecciated microfacies; (**e**) Isopachous cement and microbial spherules among dolomicrite and dolomicrosparite in the brecciated/vuggy microfacies; (**f**) network of fractures and microcavities within dolomicrite in the vuggy microfacies. Vacuolar structures are marked by a rim of dark dolomicrite and filled by equant calcite spars; (**g**) millimetric alternations of dark micrite laminae alternated with light microsparitic laminae with a dense arrangement of peloidal particles with rounded to ovoidal shape; (**h**) Micritic laminae alternated with laminae of calcite microsparite rich in peloids in the upper laminated P3 facies

detrital material mainly aligned along fractures and conduits (Fig. 5a). Detrital fraction is largely composed of quartz, K feldspar, phillites and muscovite similar to the detritus of the underlying Marnoso-arenacea turbidites. Pyrite framboids were observed as scattered aggregates, partly oxidized, or forming thin laminae which appear more frequently in the dolomicrite (Figs. 5c).

In the brecciated/vuggy microfacies, micritic clasts of various shape, commonly angular, and color (light to brown), in some cases peloidal (Fig. 5d), with a closely packed or apparently chaotic arrangements are associated to a complex reticulate of fractures and veins filled by isopachous cement made of prismatic calcite crystals with euhedral terminations and microsparite (Fig. 5e). Micritic clasts are very similar to the micritic lithotypes of the massive and laminated facies indicating derivation from the rupture of previously formed carbonate concretions. Abundant microcavities (mm to cm size) giving a "spongy" appearance are present within the cementing dolomicrite and dolomicrosparite, in some cases bordered by microbial spherules (Figs. 5e, f). Larger elongated pores and fissures are also present, oriented parallel to the bed/laminae surfaces. They are marked by a rim of dark dolomicrite and filled by equant calcite spars (Fig. 5f).

The carbonate samples from the upper laminated facies consist of millimetric-thin alternations of dark micrite with light microspar laminae, white to gray in color (Fig. 5g, h). They are predominantly composed of calcite or dolomite and calcite (Table 1). Microsparitic laminae contain abundant peloidal particles, rounded to ovoidal to elongated in shape, with a preferred orientation parallel to the surfaces of laminae. Micritic and peloidal laminae are frequently alternated with white or gray laminae in which calcite/dolomite microspar includes variable amounts of silica and clay particles.

Scanning electron microscopy (SEM) and energy dispersive spectroscopy (EDS)

The SEM-EDS analyses of three samples (PR8, PR9, PR10) from outcrop facies P1, revealed a recurring chemistry of the carbonate phases (Supplementary Information). In all the samples, we recognized a low backscatter dolomitic phase (Fig. 6) containing 30.3–71.6% m/m CaO and 20.3–44.8% m/m MgO, in contact with a higher-backscatter low-Mg calcite phase (up to 2.2% m/m MgO) (Fig. 6a, c, d). Calcite also fills fractures in the dolomite cements, indicating it formed later in the paragenetic succession. Pyrite is abundant and occurs with framboidal morphologies forming aggregates ranging in size from <5 mm to ~30 mm. Pyrite is locally distributed in a laminated fashion (Fig. 6b). Particles of barite have also been identified via SEM-EDS within the dolomite cements (Supplementary Information).

Isotope geochemistry

The stable carbon and oxygen isotopic composition of the investigated samples is highly heterogeneous, with common trends at microfacies scale. Starting from the stratigraphically lower samples (PR8, PR9 and PR10) from the brecciated facies P1, the $\delta^{13}C$ values range between −44.2‰ and −31.2‰ (Table 1; Fig. 7). We distinguished mainly 5 microfacies in these isotope investigations (Fig. 7). Overall, micrite (vuggy microfacies, light and dark micrites) has heavier $\delta^{18}O$ and slightly less negative $\delta^{13}C$ compared to the sparry and rim cements. Two micritic samples from outcrop facies 2 rich in lucinid clams yielded $\delta^{13}C$ values of −32.7‰ and −27.0‰, slightly heavier than in facies P1 (Fig. 7) and $\delta^{18}O$ values of 5.8‰ and 5.6‰. Moving stratigraphically upward, samples from the laminated facies P3 show isotopic differences depending on the type of laminae, with the ones rich in peloids having more negative $\delta^{13}C$ values than the others. The peloidal laminae show the most negative $\delta^{13}C$ values of the entire dataset ranging from −47.8‰ to −14.5‰, and $\delta^{18}O$ values between 0.8‰ to 2.7‰. Two micritic laminae show $\delta^{13}C$ values of −23.1‰ and −8.7‰ and $\delta^{18}O$ values of 3.8‰ and 4.8‰. A microsparitic laminae yielded $\delta^{13}C=-11.3$‰ and $\delta^{18}O$ = 1.8‰. Microsparitic cement in a sample collected from facies P3 has $\delta^{13}C=-34.8$‰ and $\delta^{18}O$ = -0.7‰. In general, micritic samples have heavier $\delta^{18}O$ compared to the sparry and rim cements (Fig. 7).

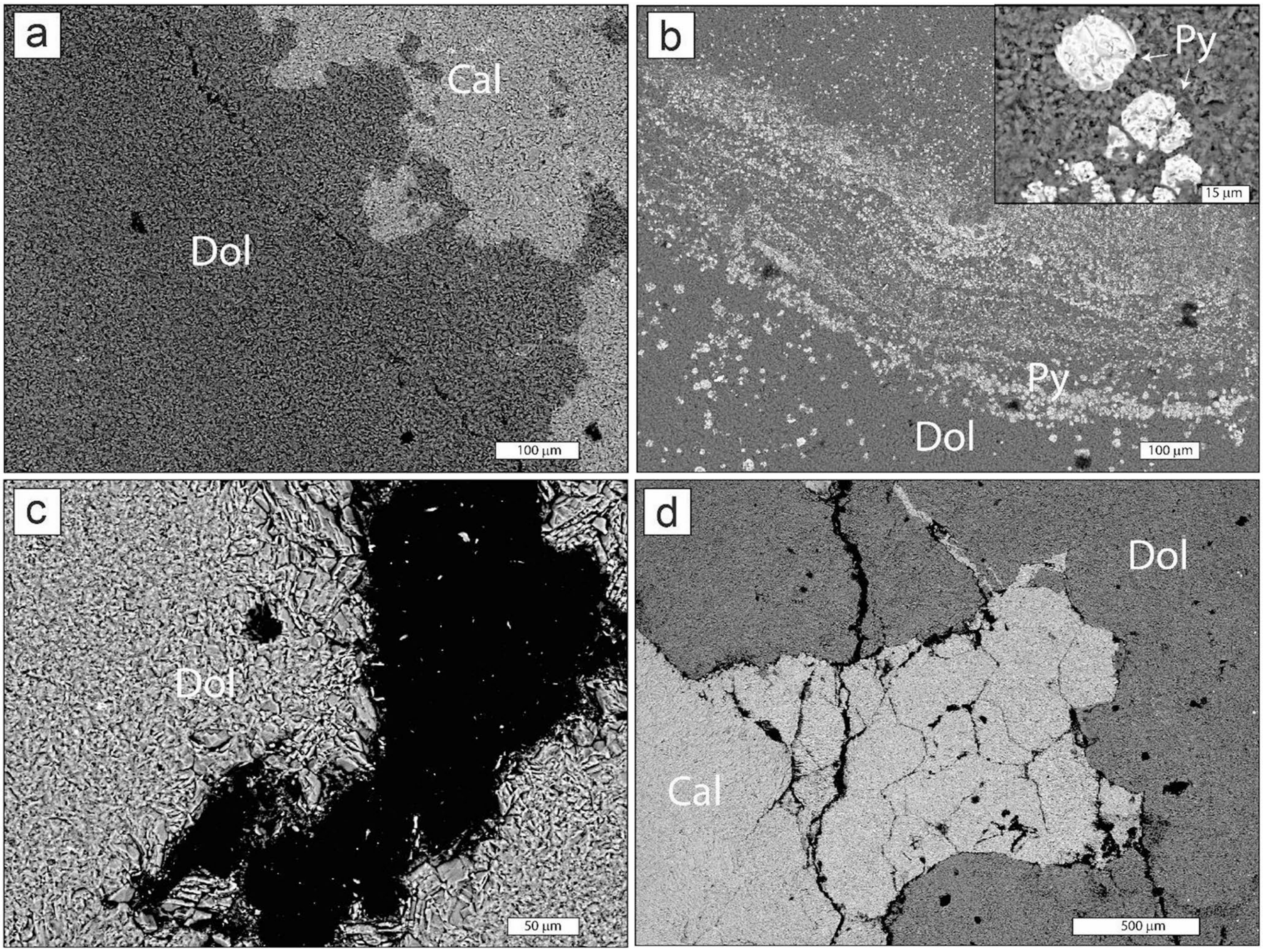

Fig. 6 Backscattered SEM images of thin sections obtained from the brecciated carbonates. Lighter colors correspond to heavier compounds. (**a**) Contact between microcrystalline dolomite and calcite phases in sample PR8. (**b**) Laminated pyrite (iron sulfide) accumulations in sample PR9. Inset shows a close-up view of pyrite framboids. (**c**) Higher magnification on dolomite cements lining a cavity in sample PR9. (**d**) Calcite and dolomite phases in sample PR10; calcite fills the fractures in the dolomite

Discussion

The studied seep-carbonate outcrop in the Predappio area are included in upper Tortonian- lower Messinian marine euxinic sediments of the Apennine foredeep (Fig. 2). These carbonates display an evident vertical trend in carbonate facies passing from brecciated carbonates dominating the lower-medium portion of the stratigraphic section to massive micritic facies rich in large bivalve mollusks and planktonic foraminifera (also found laterally to breccias) (Figs. 3 and 4) on the upper portions. The seep-related sequence ultimately evolves at the top into laminated microbial carbonates depleted in macrofauna. The microcrystalline groundmass is mostly composed of primary micrite, largely dolomitic and subordinately calcitic, and by early-diagenetic microspar cements (Fig. 5). Clasts in brecciated facies are micrites, light and dark in color. Different generations of cements fill voids and fractures, isopachous cements, dolomitic rim and later sparitic calcite filling voids (Fig. 6). The laminated deposits are mostly composed of microlaminae (prevalent calcite, subordinate dolomite) rich in peloidal particles alternated with microsparitic layers including scarce amounts of clay minerals.

The samples from our study showed wide isotopic ranges (Fig. 7): strongly depleted $\delta^{13}C$ values (−44‰ to −27‰) occur in the massive and brecciated facies, both micrite and vein cements; whereas in the upper laminated facies seep-carbonates show less depleted values in $\delta^{13}C$ (up to −8‰). The anaerobic oxidation of methane releases isotopically light dissolved inorganic carbon (DIC), which adds up to other DIC sources already present in the pore water, i.e. Late Miocene bottom seawater-derived DIC ($\delta^{13}C \sim -3.5‰$) (Sabino et al. 2022) and DIC from organic matter oxidation (>~ −25‰). AOM-derived DIC carries the composition of

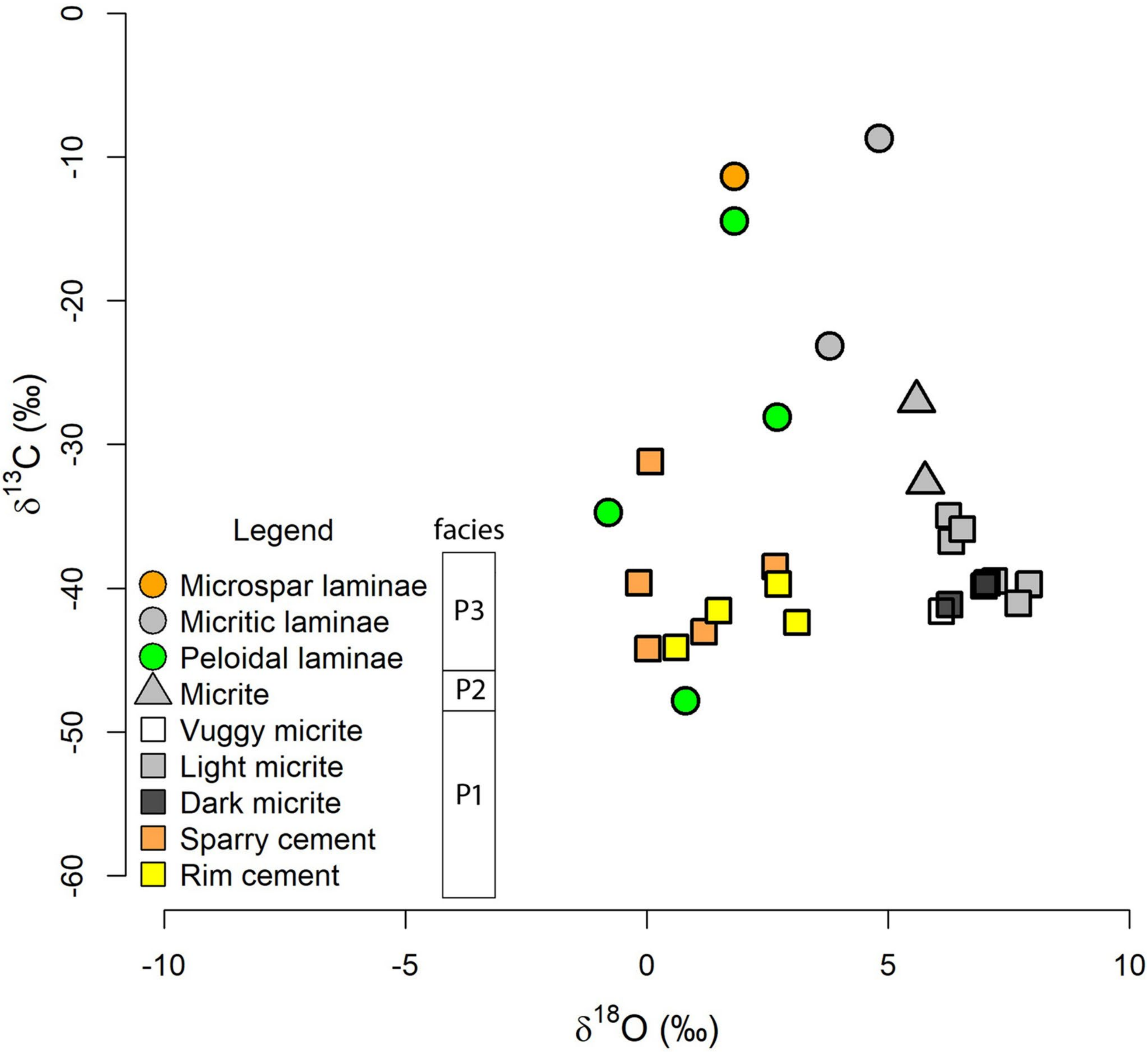

Fig. 7 Isotopic composition ($\delta^{13}C$, $\delta^{18}O$) of carbonate samples from the Predappio outcrop. Different symbols and colors refer to the major outcrop facies (Figs. 2 and 3) and microfacies identified on thin sections, respectively (Table 1)

methane being oxidized, which in turn is generally much lighter than −30‰ (Judd and Hovland 2009). Since these authigenic carbonates form in the sediment interval of highest alkalinity production by AOM, they tend to record $\delta^{13}C$ compositions < −30‰. The values measured in our samples clearly point to variable amounts of incorporation of methane-derived carbon in a methane-charged sedimentary setting.

The distribution and trend in isotope values of the different seep-carbonates are likely a consequence of variations in fluid intensity and possibly composition, with the establishment of diverse environmental settings and facies. The massive carbonate facies with large bivalves indicates a seafloor environment with low-moderate flux intensity and rates of methane oxidation. In fact, high AOM rates would generate high fluxes of HS^- toward the seafloor which can cause temporary toxic conditions for macrobenthos (Bagarinao 1992; Riesch et al. 2015) relying on well-oxygenated bottom waters for their metabolic processes. We do not have site-specific paleo-bathymetric reconstructions for this site, but the regional geology indications (Di Giulio et al. 2013) as well as the abundance of planktonic foraminifera in the samples suggest a moderately deep slope environment, approximately in the range of 500 m to 1000 m. The siliciclastic detritus dispersed in micritic carbonates and concentrated in fractures (Fig. 5a) belongs to the underlying sediments of the Marnoso-arenacea Fm confirming a fluid circulation originated from the substratum.

A dominant portion of the studied seep bodies is strongly fragmented, to form monogenic breccias with clasts made up of light and dark micrites and abundant vuggy, vacuolar and drusy fabrics. The complex alternation of overpressure phases and episodic hydrofracturing would have enlarged the conduits and dismembered the previously precipitated crusts, forming a multiple reworking of the breccias (Fig. 4c, e).

The micrite and cements are remarkably enriched in ^{18}O; in particular $\delta^{18}O$ in micrite ranges from 6‰ and 8‰. The $\delta^{18}O$ composition of authigenic carbonates forming in equilibrium with coeval seawater can be calculated by applying thermodynamic equations. Assuming an average $\delta^{18}O = -0.4$‰ (V-SMOW) (James et al. 1994; Lear et al. 2000) and bottom water temperature ~ 5 °C (Barbieri et al. 2000) we obtain values of $\delta^{18}O = 0.94$‰ for low-Mg calcite (Tarutani et al. 1969; Friedman and O'Neil 1977) and $\delta^{18}O = 3.5$‰ for dolomite (Vasconcelos et al. 2005). Therefore, the values measured in our samples are not compatible with precipitation in isotopic equilibrium with coeval seawater as they are heavier than calculated. We also rule out post-depositional diagenetic alteration, since the temperature gradients in the sedimentary column and/or meteoric weathering would alter the carbonate isotopic composition toward lighter values (negative $\delta^{18}O$), which is the opposite to what we observed.

Based on petrographic and geochemical features, we propose that studied seep-carbonates could be related to paleo-gas hydrate destabilization, similarly to other coeval outcrops of the same geographic region (Montepetra, Conti et al. 2010). Our thermodynamic model for the paleo-gas hydrate stability zone indicates that gas hydrates were stable at water depths > 480 m (Supplementary Information), which is consistent with lithological constraints imposed by our field work datasets and regional geology. We cannot exclude the contribution from deep-sourced fluids rich in ^{18}O from clay dehydration at greater depth (Kastner et al. 1991) to the observed oxygen anomalies. However, the petrographic features resembling modern clathrites (Bohrmann et al. 2002; Kennett and Fackler-Adams 2000) together with methane-related carbon isotopic signatures, strongly supports the hydrate hypothesis for the origin of the carbonates in the Predappio outcrop.

The upper portion of the examined seep-carbonate bodies exhibits sedimentological and petrographic features indicative of a microbial origin (Peckmann et al. 2004) such as laminations, peloids, elongated micritic particles and clotted micrite. As observed in other correlated outcrops (Brisighella) these characters could be interpreted as cyanobacterial (or some other bacterial) or algal origin (Conti et al. 2024). Similar to the examined features are also stromatolites from the Lower Messinian of the Calcare di Base Fm from Sicily (Oliveri et al. 2010), interpreted as *Beggiatoa*-like sulphur bacteria, as well as structures known both from modern and fossil benthic coccoidal cyanobacterial mats that underwent early mineralization (Kempe and Ka´zmierczak 1993). Yet, the $\delta^{13}C$ values as negative as −47.8‰ in peloidal laminae from this facies still point to variable amounts of incorporation of methane-derived carbon, thus suggesting methane-rich sediment conditions.

Petrographic structures and isotope compositions similar to the ones from this study have been reported from Messinian-age Monferrato (*Septarian Like-Beds* in Natalicchio et al. 2012) other than Montepetra (Conti et al. 2010). For these outcrops, the paleo occurrence of gas hydrates was established based on clathrite facies and oxygen isotope anomalies similar to modern counterparts (Greinert et al. 2001; Pierre and Rouchy 2004; Teichert et al. 2005; Bohrmann and Torres 2006; Suess 2020; Bojanowski et al. 2021). Nevertheless not all fractured seep-carbonates are related to gas-hydrate systems and some may have been sourced by deeper gas reservoirs from a secondary circuit in the Montepetra outcrop (Conti et al. 2010).

As reported in modern analogue systems in foredeep basins worldwide, the hydrate destabilization and high methane fluxes to the paleo-seafloor would have been favored by active geodynamic conditions, as occurred during the late Miocene in the Apennine foredeep affected by continuous bathymetric changes caused by the eastwardly-migrating accretionary wedge, and the complex fault-fracture system in the frontal part of the wedge provided effective migration pathways for methane-rich fluids (Argentino et al. 2019b). The lack of a precise chronostratigraphic constraint for the Predappio carbonates, established based on the age of enclosing rocks, preclude an accurate correlation with basinal structural events and sea-level changes which could have favored the gas hydrate destabilization. The future integration of other chronological methods such as U-Pb dating recently reported by Giunti et al. (2025) or Strontium Isotope Stratigraphy (Argentino et al. 2019a) could improve the resolution of our age model and allow high-resultion chronostratigraphic correlations with Miocene outcrops in this region.

Conclusions

In this study we report on a new Miocene seep-carbonate outcrop in the northern Apennines (Italy) which shows strong petrographic and geochemical evidence for paleo-gas hydrate destabilization. This outcrop is composed of carbonate bodies with stratiform to pinnacular geometries, and having thicknesses up to 30 m and lateral extent up to 100 m. The entire outcrop develops laterally over 800 m and is hosted in the late Miocene turbiditic foredeep deposits of the Marnoso-arenacea Fm. We interpreted three main carbonate facies in a stratigraphic section encompassing the seep-impacted interval. The lowermost carbonate bodies mainly consist of brecciated limestones in a micritic or sandy matrix, characterized by veins, fractures, and scarce fossil content. Moving upward, carbonates are made up of marly limestones with densely packed bivalve fossils (mostly lucinids). The uppermost carbonates show a laminated microbialite-like facies barren of macrofossils. This facies succession can be traced also within individual bodies. Stable isotope analyses on different facies revealed anomalously heavy isotope oxygen signatures (7.9‰) in the basal massive facies associated with vuggy appearance and $\delta^{13}C < -40‰$. Our thermodynamic modelling of the paleo-gas hydrate stability zone indicates that hydrates were potentially occurring at depths > 480 m, in agreement with the expected paleo-bathymetry of this slope setting. Similarly to what observed in modern analogue systems in foredeep basins worldwide, the active geodynamic conditions in the eastwardly-migrating Apennine foredeep during the Miocene would have caused hydrate destabilization and high methane fluxes to the paleo-seafloor. This process eventually resulted in the formation of widespread seep-carbonate deposits now exposed on land. This model, combined with previous studies on coeval outcrops in northern Italy, provides new insights into cold seepage dynamics in this sector of the Western Mediterranean during the stages prior to the onset of the Messinian Salinity Crisis that set the base for future high-resolution regional chronostratigraphic correlations.

Supplementary Information The online version contains supplementary material available at https://doi.org/10.1007/s00367-025-00830-8.

Acknowledgements We are grateful to Federico Lugli and Anna Cipriani (Unimore) for analytical assistance during isotope analyses and for the use of MEGIC Metallomics and Geochemistry laboratory (Unimore) tools for sample preparation. We are indebted to Chiara Fioroni for biostratigraphic indications, to Paolo Serventi (Unimore) for assistance in the field and sample collection and to Simona Marchetti Dori (Unimore) for SEM analytical assistance. We acknowledge the two anonymous reviewers and the Editor for useful feedback which improved the manuscript.

Author contributions S.M., S.C. and D.F. conceived the study, and together with C.A. they designed the experiments. S.M., S.C. and D.F. performed field work and stratigraphic logging; all the authors discussed and interpreted the microscopy and geochemistry data. S.M., S.C. and D.F. prepared Figs. 1, 2 and 3; Table 1, and C.A. prepared Figs. 4, 5, 6 and 7 and conducted thermodynamic modeling. All co-authors contributed to the manuscript.

Funding Open access funding provided by UiT The Arctic University of Norway (incl University Hospital of North Norway). This research has been founded by FAR Unimore 2024. CA position is funded by EMAN7 project (Research Council of Norway Grant No. 320100).

Data availability The authors declare that the data supporting the findings of this study are available within the paper and its Supplementary Information files.

Declarations

Competing interests The authors declare no competing interests.

References

Abegg F, Bohrmann G, Freitag J, Kuhs W (2007) Fabric of gas hydrate in sediments from the hydrate Ridge— results from ODP 204 samples. Geo Mar Lett 27:269–277

Aloisi G, Pierre C, Rouchy JM, Foucher JP, Woodside J, Scientific Party MEDINAUT (2000) Methane-related authigenic carbonates of Eastern mediterranean sea mud volcanoes and their possible relation to gas hydrate destabilization. Earth Planet Sci Lett 184:321–338

Argentino C, Lugli F, Cipriani A, Conti S, Fontana D (2019a) A deep fluid source of radiogenic Sr and highly dynamic seepage conditions recorded in miocene seep carbonates of the Northern Apennines (Italy). Chem Geol 522:135–147

Argentino C, Conti S, Fioroni C, Fontana D (2019b) Evidence for paleo-gas hydrate occurrence: what we can infer for the Miocene of the Northern Apennines (Italy). Geosciences 9(134):1–17

Argentino C, Mattingsdal R, Eidvin T, Ohm SE, Panieri G (2025) A constellation of mud volcanoes originated from a buried Arctic mega-slide, southwestern Barents Sea. Sci Rep 15(1):15161

Argnani A, Ricci Lucchi F (2001) Tertiary siliciclastic turbidite systems of the Northern apennines. In: Vai GB, Martini IP (eds) Anatomy of a mountain: the apennines and adjacent mediterranean basins. Kluwer Academic, London, pp 327–350

Bagarinao T (1992) Sulfide as an environmental factor and toxicant: tolerance and adaptations in aquatic organisms. Aquat Toxicol 24(1–2):21–62

Barbieri R, Aharon P, Taviani M, Ricci-Lucchi F, Vai GB (2000) Were Gas Hydrates Associated with Miocene-Age Cold Seeps of the Apennines? In EAGE Conference on Geology and Petroleum Geology of the Mediterranean and Circum-Mediterranean Basins. European Association of Geoscientists & Engineers, pp cp-109

Bassetti MA, Manzi V, Lugli S, Roveri M, Longinelli A, Ricci Lucchi F, Barbieri M (2004) Paleoenvironmental significance of

Messinian post-evaporitic lacustrine carbonates in the Northern Apennines, Italy. Sediment Geol 172:1–18

Boetius A, Ravenschlag K, Schubert CJ, Rickert D, Widdel F, Gieseke A, Amann R, Jørgensen BB, Witte U, Pfannkuche O (2000) A marine microbial consortium apparently mediating anaerobic oxidation of methane. Nature 407:623–626

Bohrmann G, Torres ME (2006) Gas hydrates in marine sediments. Marine geochemistry Berlin. Springer Berlin Heidelberg, Heidelberg, pp 481–511

Bohrmann G, Heeschen K, Jung C, Weinrebe W, Baranov B, Cailleau B, Heath R, Hühnerbach V, Hort M, Masson D, Trummer I (2002) Widespread fluid expulsion along the seafloor of the Costa Rica convergent margin. Terra Nova 14(2):69–79

Bojanowski MJ, Oszczypko-Clowes M, Barski M, Oszczypko N, Radzikowska M, Ciesielska Z (2021) Slope destabilization provoked by dissociation of gas hydrates in the outer Carpathian basin during the oligocene: sedimentological, petrographic, isotopic and biostratigraphic record. Mar Pet Geol 123:104585

Bonini M (2006) Detachment folding–related miocene submarine slope instability in the Romagna Apennines (Italy). J Geophys Res Solid Earth 111:b01404

Campbell KA (2006) Hydrocarbon seep and hydrothermal vent paleoenvironments and paleontology: past developments and future research directions. Palaeogeogr Palaeoclimatol Palaeoecol 232(2–4):362–407

Cochran JK, Landman NH, Jakubowicz M, Brezina J, Naujokaityte J, Rashkova A, Garb MP, Larson NL (2022) Geochemistry of cold hydrocarbon seeps: an overview. In: Kaim A, Cochran JK, Landman NH (eds) Ancient hydrocarbon seeps. Springer, pp 3–45

Conti S, Fontana D, Lucente CC (2008) Sedimentary filling of a wedge-top basin and relationship with the foredeep (Middle Miocene Marnoso-arenacea formation. North Apennines). Facies 54:479–498

Conti S, Fontana D, Mecozzi S, Panieri G, Pini GA (2010) Late Miocene seep-carbonates and fluid migration on top of the Montepetra intrabasinal high (Northern Apennines, Italy): relations with synsedimentary folding. Sediment Geol 231:41–54

Conti S, Fioroni C, Fontana D, Grillenzoni C (2016) Depositional history of the Epiligurian wedge-top basin in the Val Marecchia area (northern Apennines, Italy): a revision of the Burdigalian-Tortonian succession. Ital J Geosci 135(2):324–335

Conti S, Argentino C, Fioroni C, Salocchi AC, Fontana D (2021) Miocene seep-carbonates of the Northern Apennines (Emilia to Umbria, Italy): an overview. Geosciences 11(53):1–17

Conti S, Argentino C, Bojanowski M, Fioroni C, Giunti S, Kremer B, Fontana D (2024) The transition from normal marine to evaporitic conditions in a cold seep environment: the Messinian succession of Northern Italy. Mar Pet Geol 160:1–15

Dela Pierre F, Martire L, Natalicchio M, Clari P, Petrea C (2010) Authigenic carbonates in upper miocene sediments of the tertiary Piedmont basin (NW Italy): vestiges of an ancient gas hydrate stability zone? Geol Soc Am Bull 122(7–8):994–1010

Di Giulio A, Mancin N, Martelli L, Sani F (2013) Foredeep paleobathymetry and subsidence trends during advancing then retreating subduction: the NorthernApennine case (Oligocene-Miocene, Italy). Basin Res 25:260–284

Dubilier N, Bergin C, Lott C (2008) Symbiotic diversity in marine animals: the art of harnessing chemosynthesis. Nat Rev Microbiol 6(10):725–740

Faccenna C, Funiciello F, Giardini D, Lucente P (2001) Episodic backarc extension during restricted mantle convection in the central mediterranean. Earth Planet Sci Lett 187:105–116

Flecker R, Krijgsman W, Capella W, de Castro Martíns C, Dmitrieva E, Mayser JP, Marzocchi A, Modestou S, Ochoa D, Simon D, Tulbure M (2015) Evolution of the late Miocene Mediterranean–Atlantic gateways and their impact on regional and global environmental change. Earth-Sci Rev 150:365–392

Friedman I, O'Neil JR (1977) Compilation of Stable Isotope Fractionation Factors of Geochemical Interest. U.S. Geol. Surv. Professional Paper 440-KK, Data of Geochemistry, 6th Edition, Chapter KK, KK1-KK12

Giunti S, Mottram C, Natalicchio M, Martire L, Chapman G, Dela Pierre F, Bojanowski MJ (2025) Using U-Pb dating of cenozoic seep carbonates to assess periods of hydrocarbon seepage in sedimentary basins. Chem Geol 69X:123016

Greinert J, Bohrmann G, Suess E (2001) Methane-venting and gas hydrate-related carbonates at the Hydrate Ridge: their classification, distribution and origin. In: Paull CK, Dillon WP (Eds.) Natural Gas Hydrates: Occurrence, Distribution, and Detection. Geophysical Monograph 124:99–113

Guido A, Jacob J, Gautret P, Laggoun-Défarge F, Mastandrea A, Russo F (2007) Molecular fossils and other organic markers as palaeoenvironmental indicators of the Messinian calcare di base formation: normal versus stressed marine deposition (Rossano Basin, Northern Calabria, Italy). Palaeogeogr Palaeoclimatol Palaeoecol 255:265–283

Han X, Suess E, Liebetrau V, Eisenhauer A, Huang Y (2014) Past methane release events and environmental conditions at the upper continental slope of the South China Sea: constraints by seep-carbonates. Int J Earth Sci 103:1873–1887

Ho S, Cartwright JA, Imbert P (2012) Vertical evolution of fluid venting structures in relation to gas flux, in the Neogene–Quaternary of the lower congo Basin, offshore Angola. Mar Geol 332–334:40–55

Hryniewicz K (2022) Ancient Seep-carbonates: from outcrop appearance to microscopic petrography. In: Kaim A, Cochran JK, Landman NH (eds) Ancient hydrocarbon Seeps, topics in geobiology. Springer, pp 79–112

Jakubowicz M, Kiel S, Goedert JL, Dopieralska J, Belka Z (2020) Fluid expulsion system and tectonic architecture of the incipient Cascadia convergent margin as revealed by Nd, Sr and stable isotope composition of mid-Eocene methane seep-carbonates. Chem Geol 558:119872

James CZ, Lowell DS, Lohmann KC (1994) Evolution of early Cenozoic marine temperatures. Paleoceanography 9:353–387

Judd A, Hovland M (2009) Seabed fluid flow: the impact on geology, biology and the marine environment. Cambridge University Press, p 492

Kastner M, Elderfield H, Martin JB (1991) Fluids in convergent margins: what do we know about their composition, origin, role in diagenesis and importance for oceanic chemical fluxes? Philos Trans R Soc Lond A 335:243–259

Kempe S, Ka´zmierczak J (1993) Satonda crater lake, Indonesia: hydrogeochemistry and bio-carbonates. Facies 28:1–32

Kennett JP, Fackler-Adams BN (2000) Relationship of clathrate instability to sediment deformation in the upper neogene of California. Geology 28(3):215–218

Le Breton E, Handy MR, Molli G, Ustaszewski K (2017) Post-20 Ma motion of the Adriatic plate: new constraints from surrounding orogens and implications for crust-mantle decoupling. Tectonics 36:3135–3154

Lear CH, Elderfield H, Wilson PA (2000) Cenozoic deep-sea temperatures and global ice volumes from Mg/Ca in benthic foraminiferal calcite. Science 287(5451):269–272

Levin LA (2005) Ecology of cold seep sediments: interactions of fauna with flow, chemistry and microbes. Oceanography and marine biology. Ann Rev 43:1–46. (pp. 11-56). CRC Press.

Loher M, Marcon Y, Pape T, Römer M, Wintersteller P, Santos Ferreira C, Praeg D, Torres M, Sahling H, Bohrmann G (2018) Seafloor sealing, doming, and collapse associated with gas seeps and

authigenic carbonate structures at Venere mud volcano, Mediterranean. Deep Sea Res Part I Oceanogr Res Pap 137:76–96
Loyd SJ, Sample J, Tripati RE, Defliese WF, Brooks K et al (2016) Methane seep-carbonates yield clumped isotope signatures out of equilibrium with formation temperatures. Nat Commun 7:12274
Luff R, Wallmann K (2003) Fluid flow, methane fluxes, carbonate precipitation and biogeochemical turnover in gas hydrate-bearing sediments at Hydrate Ridge, Cascadia margin: numerical modeling and mass balances. Geochim Cosmochim Acta 67(18):3403–3421
Luff R, Wallmann K, Aloisi G (2004) Numerical modeling of carbonate crust formation at cold vent sites: significance for fluid and methane budgets and chemosynthetic biological communities. Earth Planet Sci Lett 221:337–353
Lugli S, Bassetti MA, Manzi V, Barbieri M, Longinelli A, Roveri M, Ricci Lucchi F (2007) The Messinian Vena del Gesso evaporites revisited: isotopic and organic matter characterization. In: Schreiber BC, Lugli S, Babel M (Eds.). Evaporites through space and time. Journal of the Geological Society of London 285:143–154
Naehr TH, Eichhubl P, Orphan J, Hovland M, Paull CK, Ussler W, Lorenson TD, Greene HG (2007) Authigenic carbonate formation at hydrocarbon seeps in continental margin sediments: a comparative study. Deep Sea Res Part II Top Stud Oceanogr 54(11–13):1268–1291
Natalicchio M, Birgel D, Dela Pierre F, Martire L, Clari P, Spötl C, Peckmann J (2012) Polyphasic carbonate precipitation in the shallow subsurface: insights from microbially-formed authigenic carbonate beds in upper miocene sediments of the tertiary Piedmont basin (NW Italy). Palaeogeography Palaeoclimatology Palaeoecology 329:158–172
Oliveri E, Neri R, Bellanca A, Riding R (2010) Carbonate stromatolites from a Messinian hypersaline setting in the Caltanissetta Basin, Sicily: petrographic evidence of microbial activity and related stable isotope and rare Earth element signatures. Sedimentology 57:142–161
Panieri G, Argentino C, Savini A, Ferré B, Hemmateenejad F, Eilertsen HM, Mattingsdal R, Ramalho SP, Eidvin T, Youngs S, Colson BC, Michel APM, Kapit JA, Swanborn D, Rogers AD, Angeles IB, Polteau S, Kalenitchenko D, Buenz S, Mazzini A (2025) Sanctuary for vulnerable Arctic species at the borealis mud volcano. Nat Commun 16:504
Peckmann J, Thiel V (2004) Carbon cycling at ancient methane-seeps. Chem Geol 205:443–467
Peckmann J, Thiel V, Reitner J, Taviani M, Aharon P, Michaelis W (2004) A microbial mat of a large sulfur bacterium preserved in a miocene methane-seep limestone. Geomicrobiol J 21:247–255
Pierre C, Rouchy JM (2004) Isotopic compositions of diagenetic dolomites in the tortonian marls of the Western mediterranean margins: evidence of past gas hydrate formation and dissociation. Chem Geol 205(3–4):469–484
Riesch R, Tobler M, Plath M (2015) Hydrogen sulfide-toxic habitats. Extremophile fishes: ecology, evolution, and physiology of teleosts in extreme environments, pp.137–159
Roberts HH (2001) Fluid and gas expulsion on the Northern Gulf of Mexico continental slope: mud-prone to mineral-prone responses. In: Paull CK, Dillon WP (Eds.), Natural Gas Hydrates: Occurrence, Distribution, and Detection. American Geophysical Union Geophysical Monograph Series, Washington DC 124:145–161
Sabino M, Birgel D, Natalicchio M, Pierre FD, Peckmann J (2022) Carbon isotope excursions during the late miocene recorded by lipids of marine *Thaumarchaeota*, Piedmont Basin, mediterranean sea. Geology 50(1):32–36
Serov P, Vadakkepuliyambatta S, Mienert J, Patton H, Portnov A, Silyakova A, Panieri G, Carroll ML, Carroll J, Andreassen K, Hubbard A (2017) Postglacial response of Arctic Ocean gas hydrates to climatic amelioration. Proc Natl Acad Sci U S A 114(24):6215–6220
Sloan ED (2006) Clathrate hydrates of natural gases. Chemical Industries/119. CRC
Suess E (2020) Marine cold seeps: background and recent advances. Hydrocarbons, oils and lipids: Diversity, origin, chemistry and fate, 747–767
Taludaker AR (2012) Review of submarine cold seep plumbing systems: leakage to seepage and venting. Terra Nova 24:255–272
Tarutani T, Clayton RN, Mayeda TK (1969) The effect of polymorphism and magnesium substitution on oxygen isotope fractionation between calcium carbonate and water. Geochim Cosmochim Acta 33(8):987–996
Teichert BMA, Torres ME, Bohrmann G, Eisenhauer A (2005) Fluid sources, fluid pathways and diagenetic reactions across an accretionary prism revealed by Sr and B geochemistry. Earth Planet Sci Lett 239(1–2):106–121
Terzi C, Lucchi FR, Vai GB, Aharon P (1994) Petrography and stable isotope aspects of cold-vent activity imprinted on Miocene-age calcari a Lucina from Tuscan and Romagna Apennines, Italy. Geo-Mar Lett 14:177–184
Tong H, Wang Q, Peckmann J, Cao Y, Chen L, Zhou W, Chen D (2016) Diagenetic alteration affecting δ18O, δ13C and 87Sr/86Sr signatures of carbonates: a case study on cretaceous seep deposits from Yarlung-Zangbo suture Zone, Tibet, China. Chem Geol 444:71–82
Vadakkepuliyambatta S (2019) A graphical user interface for estimating the gas hydrate stability in marine sediments repository: https://dataverse.no/dataset.xhtml?persistentId=doi:10.18710/OIXJEK
Vasconcelos C, McKenzie JA, Warthmann R, Bernasconi SM (2005) Calibration of the δ18O paleothermometer for dolomite precipitated in microbial cultures and natural environments. Geology 33(4):317–320
Weber T, Wiseman NA, Kock A (2019) Global ocean methane emissions dominated by shallow coastal waters. Nat Commun 10(1):4584